Journal of Engineering Technology and Applied Physics

An Analysis of Split-Ring Resonators and Potential Barcode Application

Chu Shen Ong[1,*], Kim Ho Yeap[1], Zhi Lin Chong[2] and Humaira Nisar[2]
[1]*Centre for Photonics and Advanced Materials Research, Universiti Tunku Abdul Rahman, 31900 Kampar, Perak. Malaysia.*
[2]*Dept. of Electronic Engineering, Faculty of Engineering and Green Technology, Universiti Tunku Abdul Rahman, 31900 Kampar, Perak, Malaysia.*
[*]*Corresponding author*: chushen96@1utar.my, *ORCiD*: 0009-0000-1489-826X
https://doi.org/10.33093/jetap.2024.6.1.10
Manuscript Received: 16 October 2023, Accepted: 18 November 2023, Published: 15 March 2024

***Abstract* — This paper presents an analysis of various split-ring resonator (SRR) configurations coupled with coplanar waveguides (CPW). Three distinct resonant structures are presented, namely, the S-shaped split-ring resonator (S-SRR), the conventional split-ring resonator (SRR), and a pair of SRR. Among the examined resonant structures, it is observed that the S-SRR exhibits the smallest electrical size with the corresponding resonant frequency of 1.37 GHz, while the conventional SRR has the largest electrical size with the corresponding resonant frequency of 3.34 GHz. On the other hand, the resonant frequency of a dual SRR is 2.37 GHz. However, the transmission coefficient of a dual SRR is -11.43 dB, which is higher than S-SRR (-10.02 dB) and SRR (-8.18 dB). Furthermore, this study extends the analysis between a square dual SRR and a circular dual SRR with retained area. The square SRR demonstrates a lower resonance frequency (2.23 GHz) relative to its circular counterpart (2.37 GHz). The comparison also shows that the transmission coefficient of the square configuration is -13.88 dB, which is higher than its circular counterpart (-11.43 dB). The realization of a barcode application is achieved by loading multiple S-shaped split ring resonators (S-SRRs) with varying geometric parameters adjacently onto the transmission line. By individually rotating each of these S-SRRs, it becomes possible to alter the notch magnitude, thereby positioning it within a specific designated range corresponding to a particular code. In the case of a configuration involving rotations of (0°, 45°, 90°, 0°, 45°, 90°), this approach results in the creation of a barcode denoted as "100 010 000 100 011 000". This methodology enables the encoding of information in the form of distinctive resonant responses, providing a versatile and compact means of realizing barcode applications.**

Keywords*— *Split ring resonator (SRR), S-shaped split ring resonator (S-SRR), Resonance frequency, Square SRR, Metamaterials

I. INTRODUCTION

Metamaterials are composite materials that are engineered to exhibit properties that are not found in naturally occurring substances. These properties typically emerge from carefully designed structures. The development of metamaterials that can exhibit negative permeability (μ) and permittivity (ε) has been gaining interest since a split-ring resonator-based left-handed transmission line was proposed in 2003 by Martin *et al.* [1]. The coplanar waveguide (CPW) coupled to split-ring resonators (SRR) and periodically loaded with narrow metallic wires allows the negative wave to propagate in a narrow frequency band. Among the diverse range of metamaterials, double-negative media have emerged as a focal point of research in recent years. Due to the compact size of the SRR, the design of very compact microwave circuits is gaining popularity. These circuits include filters [2-4], sensors [5-7], and antennas [8]. Among different types of SRR, the S-shaped split ring resonator is gaining popularity due to the level of miniaturization that can be achieved by modifying a conventional SRR structure [3]. By modifying the original topology of the SRR, the electrical size of the SRR can be reduced, some examples of which are the spiral resonator (SR) [9] and the multiple split ring resonator (MSRR) [10].

The SRR is composed of a pair of metal rings etched in a dielectric substrate with gaps in them at opposite ends. The SRR can be excited by the time-varying magnetic field in the direction orthogonal to the symmetry plane of the resonant particle [11]. When the external magnetic field is applied, electromotive force (EMF) is induced around the SRR. The gaps in the metal rings help in obtaining a resonant structure. The S-shaped SRR, or S-SRR, is modified from the conventional SRR. It is named as such since the structure resembles the letter "S" The S-SRR does

Published by MMU PRESS. URL: https://journals.mmupress.com/index.php/jetap/index

not exhibit a symmetry plane like the SRR. However, the S-SRR can be excited by contra-directional magnetic fields, and this phenomenon engenders the generation of current flowing in the same direction [12].

The operating resonance frequency range of SRR and S-SRR depends on the geometrical dimensions and the materials used in the construction. S-SRR is able to achieve a higher level of miniaturization as compared to SRR, which makes S-SRR more suitable for compact devices. The size of the SRR is limited by the wavelength of the resonance frequency. The resonant frequency of the SRR is dependent on the LC values, which are determined by the dimensions of the SRRs. This limits the achievable resonance frequency range of the SRR in various applications, such as filters and antennas. Different resonator types are analysed to determine the application of the different resonators in a suitable frequency range due to fabrication and size limitations.

In this paper, the resonance frequency and the magnitude of transmission zero of various structures of split-ring resonators are compared and analysed; the configurations include S-shaped split-ring resonators (S-SRR), circular and square split-ring resonators (SRR), and paired circular SRR.

II. DESIGN

A. Coplanar Waveguide (CPW)

In this paper, the FR4 substrate, with a dielectric constant (ε_r) of 4.4, dielectric thickness h = 0.8 mm, and copper thickness of 35 μm, has been selected for the designs. The resonators are loaded with a coplanar waveguide (CPW) transmission line, which is printed at the top layer of the substrate. For our case, the CPW has a width (w) of 6 mm for the strip, and the ground planes and the strip are separated by a gap (g) of 0.45 mm. To match the impedance of the connectors, the characteristic impedance of the CPW is set to be 50 Ω.

B. Dual Split-Ring Resonator (SRR)

The different types of split-ring resonators are loaded at the back substrate of the CPW. Figure 1 shows the schematic view of a circular SRR.

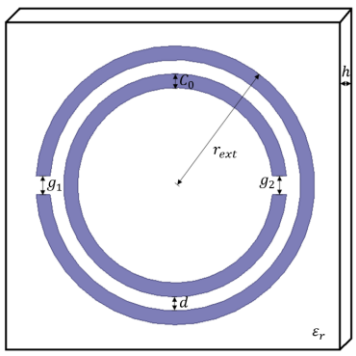

Fig. 1. The schematic view of a circular SRR, comprising an external radius, r_{ext}, ring width, c_0, dielectric spacing, d between the inner and outer rings and split gaps, g_1 and g_2.

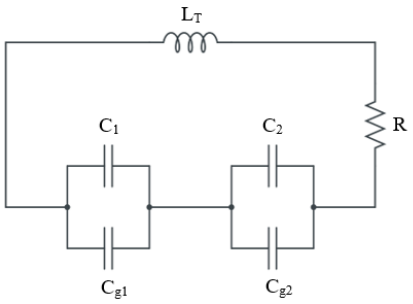

Fig. 2. The equivalent circuit of the SRR.

Figure 2 shows the lumped equivalent circuit of the SRR structure [13]. Here, L_T and C_{eq} represent, respectively, the total equivalent inductance and the total equivalent capacitance of the SRR coupled with the CPW.

The simplified expression of the total equivalent inductance, L_T for a wire with a rectangular cross section of finite length, l and thickness, c is given as [13].

$$L_T = 0.0002l(2.303 \log_{10} \frac{4l}{c} - \gamma)\ \mu H \quad (1)$$

The constant γ = 2.451 for the wire loop of the circular geometry. The wire length, l is given in Eq. (2) below [13]

$$l = 2\pi r_{ext} - g \quad (2)$$

, which is the circumference of the circular loop with the gap. The average ring radius, r_0 of the circular SRR is expressed in Eq. (3) [13].

$$r_0 = r_{ext} - c - \frac{d}{2} \quad (3)$$

The total equivalent capacitance, C_{eq} of the SRR can be found by applying (4)

$$C_{eq} = \frac{(C_0 + C_g)}{4} \quad (4)$$

Here, the gaps of the inner and outer rings are of identical dimension, $g_1 = g_2$. Thus, the gap capacitance of the ring, $C_{g1} = C_{g2} = C_g$ and the series capacitance is $C_1 = C_2 = C_0$. Both C_g and C_0 are given as [13]

$$C_g = \frac{\varepsilon_0 ct}{g} \quad (5)$$

$$C_0 = (\pi r_0 - g)C_{pul} \quad (6)$$

where C_{pul} is the capacitance per unit length and is expressed as

$$C_{pul} = \frac{\sqrt{\varepsilon_e}}{c_0 Z_0} \quad (7)$$

where, $c_0 = 3 \times 10^8$ m/s is the velocity of light, Z_0 is the characteristic impedance and ε_e is the effective permittivity of the medium. The effective permittivity is described as the composite permittivity of a material. It characterized how the overall permittivity of the material is affected by the properties of the constituent material.

C. S-Shaped Split-Ring Resonator (S-SRR)

The schematic of the S-shaped split ring resonators (S-SRR) is shown in Fig. 3. The S-SRR is formed by routing a singular metallic ring with radius, r and width, c in circular form. The upper and lower loops are separated by distance, s and both loops are connected at the center of the structure with a gap, g in between. The equivalent circuit model for the S-SRR-loaded coplanar waveguide transmission line and its transformed model are given in Fig. 4 [14].

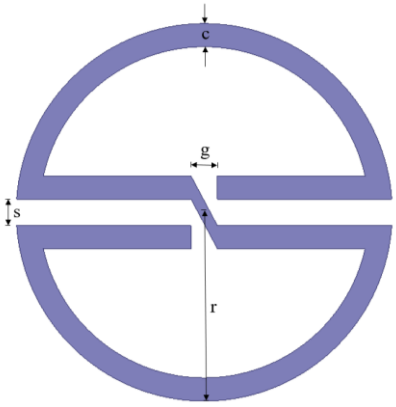

Fig. 3. The schematic view of an S-SRR with radius r, width c, spacing s between the upper and lower loops with gap g at the center of the structure.

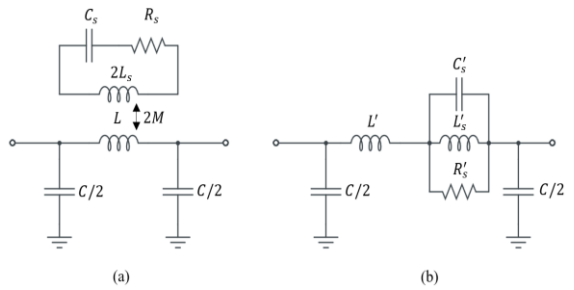

Fig. 4. The equivalent circuit of an (a) S-SRR loaded with a CPW transmission line and its (b) transformed model.

In Fig. 4, L and C represent, respectively, the inductance and the capacitance of the CPW. The inductance and capacitance of each loop of the S-SRR are denoted, respectively, L_s and C_s. The mutual inductance, $2M$ arises from the coupling between the CPW and the S-SRR, whereas the resistive loss is given as R_s. In order to simplify the analysis of the circuit, the lumped elements at the transmission line and the resonators are integrated, as depicted in Fig. 4(b). The lumped inductance L_s', capacitance C_s', and resistance R_s' of the transformed model can be computed based on Eqs. (8) to (11) below [14]

$$L_s' = \frac{M^2}{2L_s} \quad (8)$$

$$L' = L - L_s' \quad (9)$$

$$C_s' = \frac{4L_s^2 C_s}{M^2} \quad (10)$$

$$R_s' = \frac{M^2}{2L_s C_s R_s} \quad (11)$$

Since the resonance frequency f_0 of a typical LC circuit can be expressed in terms of the inductance L and capacitance C as,

$$f_0 = \frac{1}{2\pi\sqrt{LC}} \quad (12)$$

Since f_0 of the conventional SRR can be determined by substituting Eqs. (1) and (4) into L and C of Eq. (12) below and, likewise, f_0 of the S-SRR can be obtained when $L = L_s$ and $C = C_s$.

D. Different Split-Ring Resonators Loaded on the CPW Transmission Line

Different configurations of the SRR are loaded on the transmission line, as shown in Fig. 5. In Fig. 5(a), the S-SRR is constructed with a radius, r = 6.0 mm, width, c = 1.0 mm, gap, s = 1.0 mm and the gap at the center of the S-SRR, g of 1.0 mm. The circular single and paired SRRs in Fig. 5(b) and (c), on the other hand, constitute an external radius, r_{ext} = 6.0 mm and the width of the ring, C_0 = 1.0 mm. The gap between the inner ring and the outer ring of the SRR, d = 1.0 mm and the split gaps of the inner and outer ring are 1.0 mm. As can be clearly seen in Fig. 5(c), both SRRs are closely collocated, with the split gaps of the outer rings facing each other. The rings are arranged as such because the splits in the opposite directions tend to minimize the effect of electric polarizability [15].

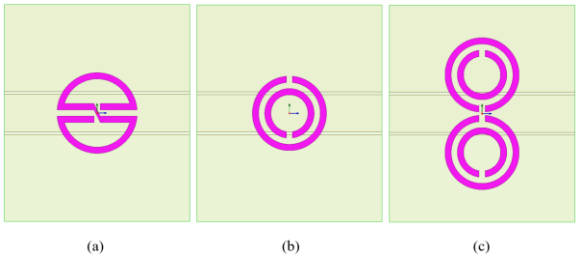

Fig. 5. The transmission line loaded with (a) a S-SRR, (b) a conventional SRR and (c) a pair of SRR.

E. Square and Circular Dual SRR

Figure 6 shows an analysis between two distinct split ring resonator (SRR) configurations, namely the square and circular SRRs, both designed to have

identical circumference. The circular dual SRR has a radius of 6.0 mm; while its square counterpart has a length and width of 10.6 mm. The area is held constant while the geometrical shape of the resonator is varied, allowing a systematic exploration of the characteristics of the behavior exhibited by these two SRR configurations.

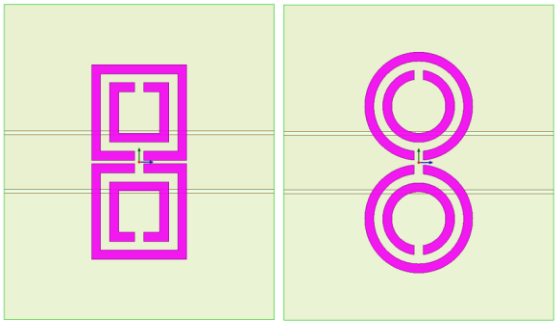

(a) (b)

Fig. 6. The transmission line loaded with (a) a square dual SRR and (b) a circular dual SRR.

III. RESULTS AND DISCUSSIONS

In order to facilitate a comparative analysis of the miniaturization capabilities among various topological configurations of the split-ring resonators (SRRs), the transmission coefficient was simulated via the ANSYS High-Frequency Structure Simulator (HFSS). Figure 7 shows the transmission coefficients generated from the S-SRR, SRR, and paired SRR. As depicted in Fig. 7, the S-SRR clearly shows the lowest resonance frequency of 1.37 GHz. In contrast, the singular SRR configuration exhibits the highest resonance frequency at 3.34 GHz. The low resonance frequency exhibited by the S-SRR can be attributed to the increase in inductance and capacitance of the S-SRR topology. This also indicates that a high level of miniaturization can be achieved by modifying the resonator shape to an S-shaped split-ring resonator [16]. This allows the S-SRR to operate at a much lower frequency. Furthermore, Fig. 7 shows that by employing a dual SRR arrangement, a substantial reduction in the resonance frequency is observed. The resonance frequency of the dual SRR arrangement is notably lowered to 2.37 GHz. It is apparent that the S-SRR configuration offers significantly smaller electrical sizes than the SRR configuration since the sizes of both structures are identical. However, as the pursuit of enhanced resonance frequency reduction and notch magnitude amplification persists, the dual SRR configuration assumes a pivotal role. In Fig. 7, the transmission coefficient of the dual SRR is -11.43 dB, which is higher than the S-SRR (-10.02 dB) and the SRR (-8.18 dB) configurations. The S-SRR can be excited by the contra-directional magnetic fields. Because of the characteristic S-shaped structure, the generated current flows in the same direction if it is properly oriented [5]. This results in a very small electrical size as compared to the paired SRR and, let alone, the single SRR configuration.

In Fig. 8, the transmission coefficients between the square and circular SRRs are compared. Clearly, the simulated resonance frequency of the square SRR is lower than that of its circular counterpart. This indicates that, for a fixed resonator area, the square SRR exhibits a smaller electrical size as compared to its circular counterpart. Further analysis of Fig. 8 reveals that the square dual SRR exhibits a notable notch depth of -13.88 dB at a resonance frequency of 2.23 GHz. In contrast, the circular dual SRR demonstrates a somewhat lower notch depth of -11.43 dB at a resonance frequency of 2.37 GHz. Maintaining the same area size, it is evident that the square dual SRR is better suited for compact design due to its smaller electrical size when compared to the circular dual SRR. The advantage of a smaller electrical size in the square dual SRR configuration is also reflected in its lower operating frequency. This characteristic offers the potential to avoid high-frequency applications, which are typically associated with higher costs.

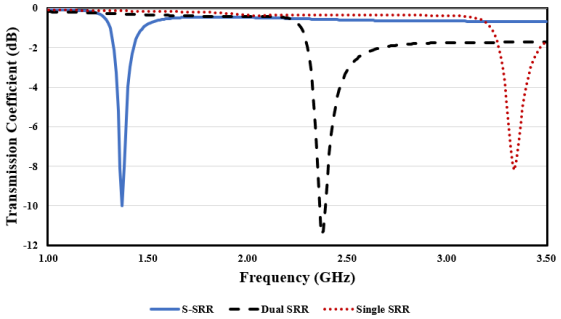

Fig. 7. The transmission coefficients of three different SRR-loaded CPW structures – namely, the S-SRR, conventional SRR and paired SRR.

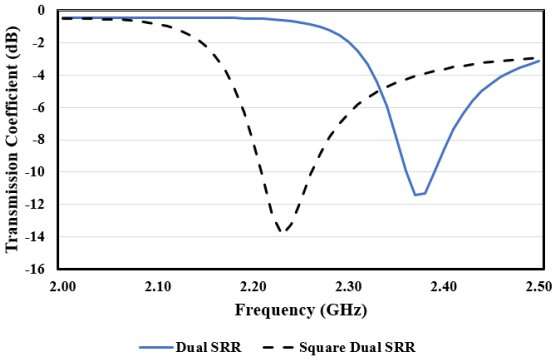

Fig. 8. The transmission coefficients of a square and a circular SRR loaded with the CPW.

IV. POTENTIAL BARCODE APPLICATION BASED ON S-SRR

To validate the feasibility of employing the S-shaped split ring resonator (S-SRR) in barcode applications, multiple multistate S-SRRs can be arranged adjacently [14]. Various S-SRR designs with distinct dimensions have been loaded onto the transmission line. The manipulation of S-SRR dimensions leads to variations in its inductance and capacitance, consequently enabling the adjustment of resonance frequencies in accordance with Eq. (12). In Fig. 9, a visual representation is provided, illustrating the arrangement of multiple S-SRR designs side by side, each possessing different dimensions. This

strategic configuration showcases the adaptability and versatility of the S-SRR in barcode realization, where diverse resonance frequencies are achieved by tailoring the S-SRR's geometric parameters [14]. In Fig. 10, the transmission coefficient of six S-SRR-loaded CPW is shown. Each of the peaks represents the resonance frequency of a single S-SRR, as shown in Fig. 9. The manipulation of S-SRR dimensions leads to variations in its inductance and capacitance, consequently enabling the adjustment of resonance frequencies in accordance with Eq. (12). By positioning six S-SRRs with different geometrical parameters that correspond to different resonance frequencies on the back substrate of CPW, six peaks can be observed, as shown in Fig. 10.

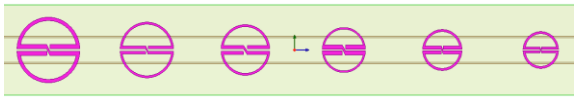

Fig. 9. The transmission line loaded with six S-SRR designs with different dimensions.

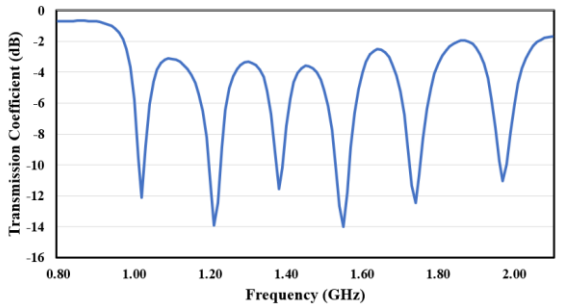

Fig. 10. The transmission coefficient of six S-SRRs loaded CPW structures.

In Table I, we have documented the resonance frequency and the corresponding transmission coefficient for each of the S-shaped split ring resonator (S-SRR) designs. As observed in the table, varying the dimensions of the S-SRR results in different resonance frequencies and transmission coefficients. This variability becomes the foundation for creating the S-SRR barcode system. Figure 11 illustrates the application of this concept, where a 3-bit code can be assigned to specific ranges. As in Table II, state "000" can be assigned for the peak located between -2.5 dB and 0 dB range; state "001" corresponds to the peak located at between -5.0 dB and -2.5 dB; state “010” corresponds to the peak located at between -7.5 dB and -5.0 dB; state “011” corresponds to the peak located at between -10.0 dB and -7.5 dB; and state “100” corresponds to the peak located at between -12.5 dB and -10.0 dB. This method of assigning states to resonance peaks provides a systematic means of realizing an S-SRR barcode system, where the encoded information is based on the distinctive resonance characteristics of each S-SRR configuration.

In Figure 12, a configuration involving rotations of (0°, 45°, 90°, 0°, 45°, 90°) is presented. This rotation of the S-shaped split ring resonator (S-SRR) between 0° and 90° results in a frequency response that is contingent on the coupling level between the transmission line and the S-SRR, determined by the angle of rotation of the S-SRR [11]. In Fig. 13, the transmission coefficient of each of the peaks is recorded in Table III. The resonance particle is excited by the magnetic field lines generated by the CPW, which have opposite directions in the upper and lower loops of the S-SRR. By rotating the S-SRR, the cancellation of the magnetic field components in the S-SRR occurs. Thus, the maximum coupling between the S-SRR and the CPW arises when $\theta = 0°$, and the minimum coupling occurs when $\theta = 90°$. The obtained results highlight the capability of assigning distinct codes to each S-SRR, culminating in a combined S-SRR barcode denoted as "100 010 000 100 011 000", as demonstrated in Table III. The compactness of the S-SRR, owing to its small electrical size, further facilitates the implementation of more compact designs to reduce the overall dimensions of the S-SRR-loaded transmission line.

Table I: Simulated resonance frequencies and the transmission coefficient.

S-SRR	Resonance frequency (GHz)	Transmission coefficient (dB)
S-SRR 1	1.02	-12.14
S-SRR 2	1.21	-13.93
S-SRR 3	1.38	-11.53
S-SRR 4	1.55	-14.02
S-SRR 5	1.74	-12.46
S-SRR 6	1.97	-11.06

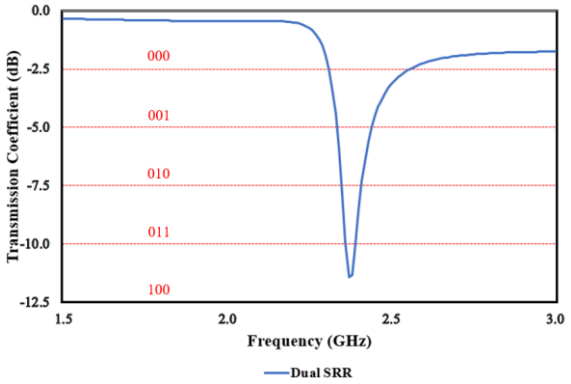

Fig. 11. State “100” is assigned to the peak lies between -12.5 dB and -10.0 dB.

Table II: Binary code assigned to a specific range of the peak of the transmission coefficients.

Transmission Coefficient (dB)	Binary Code
-2.5 to 0.0	000
-5.0 to -2.5	001
-7.5 to -5.0	010
-10.0 to -7.5	011
-12.5 to -10.0	100

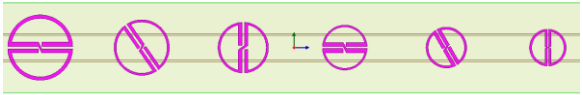

Fig. 12. The transmission line loaded with six S-SRR designs with 0°, 45°, 90°, 0°, 45°, 90°configuration.

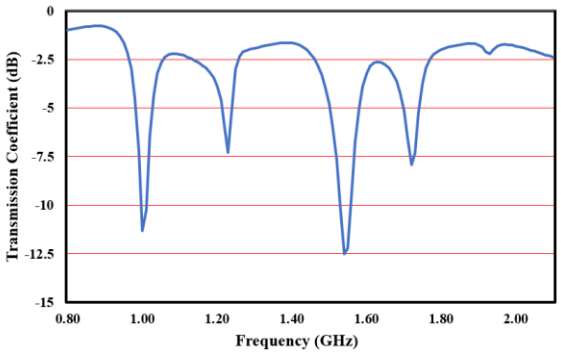

Fig. 13. The transmission coefficient of six S-SRR loaded CPW structures with 0˚, 45˚, 90˚, 0˚, 45˚, 90˚configuration.

Table III: Simulated resonance frequencies, transmission coefficient, and the binary code of each S-SRR.

S-SRR	Resonance frequency (GHz)	Transmission coefficient (dB)	Binary Code
S-SRR 1	1.00	-11.34	100
S-SRR 2	1.23	-7.28	010
S-SRR 3	1.38	-1.65	000
S-SRR 4	1.54	-12.49	100
S-SRR 5	1.72	-7.92	011
S-SRR 6	1.93	-2.21	000

V. CONCLUSION

In conclusion, this study has provided a comprehensive comparative analysis of three distinct split-ring resonator (SRR) configurations: the S-shaped split-ring resonator (S-SRR), the conventional circular and square split-ring resonators (SRRs), and the circular paired split-ring resonator. The S-SRR configuration exhibits a substantially reduced electrical size when compared to conventional SRRs. This reduction is attributed to the modification of the SRR topology, leading to increased capacitance and inductance in the S-SRR. Also, the paired SRR arrangement, despite doubling the resonator area, offers enhanced notch magnitude and a lower resonance frequency in comparison to the single SRR configuration. The comparison between the square and circular SRRs reveals that square SRRs exhibit a relatively lower resonance frequency. This is to say that the square SRR is of a smaller electrical size compared to its circular counterpart, thus rendering the square configuration a more compact and space-efficient choice. The S-SRR barcode topology is also illustrated. By having the S-SRR with different geometrical parameters and rotation angles, the barcode can be generated by assigning the code for the peak of the notch at the resonance frequency of each individual S-SRR. In summary, this comparative analysis has shed light on the diverse performance characteristics of different SRR configurations, providing valuable insights for the selection and optimization of resonant structures in various applications, particularly those where electrical size and notch magnitude are key considerations.

REFERENCES

[1] F. Martín, J. Bonache, F. Falcone, M. Sorolla and R. Marqués, "Split Ring Resonator-Based Left-Handed Coplanar Waveguide," *Appl. Phys. Lett*, vol. 83, pp. 4652-4654, 2003.

[2] C. Asci, A. Sadeqi, W. Wang, H. R. Nejad and S. Sonkusale, "Design and Implementation of Magnetically–Tunable Quad–Band Filter Utilizing Split–Ring Resonators at Microwave Frequencies," *Scientific Reports*, vol. 10, pp. 1050, 2020.

[3] A. K. Horestani, M. Durán-Sindreu, J. Naqui, C. Fumeaux and F. Martín, "Coplanar Waveguides Loaded with S-Shaped Split-Ring Resonators: Modeling and Application to Compact Microwave Filters," *IEEE Antennas Wirel. Propag. Lett.*, vol. 13, pp. 1349-1352, 2014.

[4] Z. X. Oh, K. H. Yeap, P. C. The and V. Dakulagi, "Circular Split-Ring Resonator-Based Sensor for Dielectric Constant Measurement," *Microwave Opt. Technol. Lett.*, vol. 65, pp. 513-518, 2023.

[5] J. Naqui, J. Coromina, F. Martín, A. K. Horestani and C. Fumeaux, "Comparative Analysis of Split Ring Resonators (SRR), Electric-LC (ELC) Resonators, and S-shaped Split Ring Resonators (S-SRR): Potential Application to Rotation Sensors," in *Proc. 2014 Mediterranean Microwave Symp.*, pp. 1-5, 2014.

[6] N. Alrayes and M. I. Hussein, "Metamaterial-based Sensor Design Using Split Ring Resonator and Hilbert Fractal for Biomedical Application," *Sensing and Bio-Sensing Res.*, vol. 31, 100395, 2021.

[7] J. Mata-Contreras, C. Herrojo and F. Martín, "Electromagnetic Rotary Encoders Based on Split Ring Resonators (SRR) Loaded Microstrip Lines," in *2018 IEEE/MTT-S Int. Microwave Symp*, pp. 43-46, 2018.

[8] M. Alsharari, V. Sorathiya, A. Armghan, K. Dave and K. Aliqab, "Development of Split Ring Resonator Shaped Six Element 2 × 3 Multiple Input Multiple Output Antenna for the C/X/Ku/K Band Applications," *Micromachines*, vol. 14, pp. 874, 2023.

[9] J. D. Baena, R. Marqués, F. Medina and J. Martel, "Artificial Magnetic Metamaterial Design by Using Spiral Resonators," *Phys. Rev. B*, vol. 69, pp. 0144021-0144025, 2004.

[10] F. Bilotti, A. Toscano and L. Vegni, "Design of Spiral and Multiple Split-Ring Resonators for the Realization of Miniaturized Metamaterial Samples," *IEEE Trans. Antennas Propag.*, vol. 55, pp. 2258-2267, 2007.

[11] J. Naqui, J. Coromina, A. K. Horestani, C. Fumeaux and F. Martin, "Angular Displacement and Velocity Sensors Based on Coplanar Waveguides (CPWs) Loaded with S-Shaped Split Ring Resonators (S-SRR)," *Sensors*, vol. 15, pp. 9628-9650, 2015.

[12] A. K. Horestani, N. Varmazyar, F. Sadeghikia, M. T. Noghani, Z. Shaterian and F. Martín, "On the Applications of S-shaped Split Ring Resonators (S-SRR) in Sensors, Filters, and Antennas," in *2019 Int. Conf. Electromagnetic. Adv. Appl.*, pp. 0485-0488, 2019.

[13] C. Saha and J. Y. Siddiqui, "Versatile CAD Formulation for Estimation of The Resonant Frequency and Magnetic Polarizability of Circular Split Ring Resonators," *Int. J. RF and Microwave Computer-Aided Eng.*, vol. 21, pp. 432-438, 2011.

[14] C. Herrojo, F. Paredes, J. Mata-Contreras, S. Zuffanelli and F. Martín, "Multistate Multiresonator Spectral Signature Barcodes Implemented by Means of S-Shaped Split Ring Resonators (S-SRRs)," *IEEE Trans. Microw. Theory Tech.*, vol. 65, pp. 2341-2352, 2017.

[15] A. N. Reddy and S. Raghavan, "Split Ring Resonator and Its Evolved Structures Over The Past Decade: This paper discusses the nuances of the most celebrated composite particle (split-ring resonator) with which novel artificial structured materials (called metamaterials) are built," in *IEEE Int. Conf. Emerging Trends in Comput., Commun. and Nanotechnol.*, pp. 625-629, 2013.

[16] A. K. Horestani, M. Durán-Sindreu, J. Naqui, C. Fumeaux and F. Martín, "S-Shaped Complementary Split Ring Resonators and Their Application to Compact Differential Bandpass Filters with Common-Mode Suppression," *IEEE Microwave Wirel. Compon. Lett.*, vol. 24, pp. 149-151, 2014.